UNIVERSITY OF MICHIGAN
Department of Mechanical Engineering
Cavitation and Multiphase Flow Laboratory

UMICH 014456-41-I

CAVITATION EROSION STATE OF ART AND PREDICTING CAPABILITY

(submitted for publication - Applied Mechanics Review, ASME)

by

Frederick G. Hammitt

Supported by: Office of Naval Research Contract
No. N0001 4-76-C-0697

April 25, 1979

ABSTRACT

The present state of the art concerning the basic understanding of cavitation erosion mechanisms, and the capability for "a priori" prediction of eventual cavitation erosion rates in prototype or field machines, is reviewed. Particular emphasis is given to relatively new techniques involving the measurement of pulse-height spectra from individual cavitation bubble collapses, and the correlation of these results with measured damage in both venturi and vibratory cavitation damage test devices. The concept of cavitation erosion efficiency, η_{cav} is discussed.

Best-fit correlations between material mechanical properties and cavitation resistance are briefly reviewed, indicating the best results for a linear correlation of ultimate resilience $(TS^2/2E)$ or $BHN^{1.8}$ with reciprocal maximum mean depth of penetration rate $(1/MDPR_{max})$. These would be entirely consistent, as well as dimensionally consistent, if a BHN^2 correlation were used. This relatively minor discrepancy with cavitation erosion results is not believed significant.

The use of a hypothesized "universal" damage-time curve for predictive purposes is reviewed. While this model is proven to be relatively imprecise, it may be useful in the present lack of more precise techniques.

ACKNOWLEDGMENT

Financial support for this work was provided primarily by Office of Naval Research Contract No. N00014-76-C-0697 and University of Michigan funds.

List of Figures

INTRODUCTION

Cavitation is one of the major problems confronting designers and users of modern high-speed hydrodynamic systems such as pumps of all types, marine propellors, hydraulic turbines, liquid handling valves and control devices, hydrofoils, sonar domes, and other acoustic signal devices, bearings, and diesel engine wet cylinder liners, to name only a few important examples. In general, cavitation can affect the overall component performance through various fluid dynamic effects, it can cause prohibitive noise or vibrations or other special effects, or, and perhaps most importantly, produce rapid and large-scale erosion, sometimes combined importantly with corrosion.

The state of the art of cavitation erosion was well reviewed in a 1971 article (1) in Applied Mechanics Reviews by Thiruvengadam. It is then the purpose of this article to further update the status of the cavitation erosion field, particularly with reference to "a priori" or other damage predicting techniques.

It is generally agreed that cavitation erosion is caused by the collapse of vapor bubbles entrained within the liquid at or near solid boundaries (1-5, eg.). The possibility of cavitation flows (not damage) was suggested by Euler in 1974 (1), and experiments were conducted by Reynolds in 1874 (1). A mathematical treatment was provided by Besant (1,3,5,eg) in 1869, but no engineering application was suggested. However, cavitation damage assumed engineering importance around 1900, when slow speed reciprocating marine drives were replaced by high speed

turbines, used without adequate reduction gears (2,4, eg.). This led to the establishment of a commission headed by Sir Charles Parsons (1,2) in Britain, and the pioneering analytical treatment of Rayleigh (6) in 1917, using an ideal fluid with assumed spherical symmetry. Under such conditions, infinite pressures and velocities were computed at the mathematical point of collapse and for zero time-duration. Obviously, real-fluid effects such as liquid compressibility, viscosity, "thermodynamic effects", and most importantly, the lack of spherical symmetry, moderate these infinities into finite values. However, the Rayleigh analysis (6) is extremely valuable in indicating the possibility of very high and potentially damaging pressures and velocities near the point of bubble collapse. Much analytical and numerical work has been done over the past several decades primarily to refine for real flow situations the original ideal flow analysis of Rayleigh.

II. BASIC PRINCIPLES OF CAVITATION DAMAGE

A. Generally Agreed Features

Indisputable and theoretical facts upon which the understanding of the cavitation damage mechanism must be based (4,5,eg.) are summarized next.

1) Rapid pitting and erosion often occur in flow regimes where a cavitating flow has been observed to exist, either audibly, visually, or through its effect upon flow parameters such as head or flow.

2) Such cavitating flows can, under certain circumstances, damage even the most resistent of materials, such as stellites, tool steels, or any as yet tested structural material. Such damage can occur rapidly even for liquid-material combinations

where corrosive effects should be negligible, eg., petroleum products upon glass or stainless steel. Thus the primary mechanism cannot be corrosion in many cases.

3) Cavitation damage appears to include strong components of mechanical attack, due to the observed presence of such mechanical features as surface work-hardening and slip lines. Single craters formed during the early portion of the damage (Figs. 1 & 2), are roughly symmetrical, usually with raised rim, as if formed by single impact (4,5,7, eg.) rather than corrosion. Cavitation damage thus closely resembles liquid impact damage (1-5, eg.), though on a much finer scale of pit size.

4) Mechanical cavitation and corrosion attack are strongly self-reinforcing, since mechanical attack removes protective coatings, and the resultant surface roughness creates new local cavitation.

5) The potential for extremely high liquid pressures and velocities in the vicinity of a collapsing spherical vapor-filled bubble in an inviscid, incompressible, and spherically-symmetric liquid was shown by the classical Rayleigh analysis (1-6, eg.). These expectations have been confirmed by many more recent and comprehensive analyses (8-11,eg.) for "real-fluid" conditions, to include some typical studies.

Certain conclusions can then be drawn from these generally agreed basic facts.

1. Since cavitation regimes usually contain large numbers of essentially spherical bubbles of various diameters, the individual collapse of which would create local pressures and velocities sufficient to be damaging to most materials, it is

probable that a material surface exposed to such a cavitation field will experience a multiplicity of impulses of widely varying intensities and locally random spatial distribution. The duration of such impulses is only a few μs, for typical original bubble diameter of ~1 mm. Further, the duration, impulse magnitude, and affected surface area increase with initial bubble size and/or collapsing pressure differential, i.e., "suppression pressure" = p_{sv} = static pressure - vapor pressure = $\rho \cdot$NPSH*.

Since surface impulse spectra are extensive, individual craters covering a wide range of diameters will be formed (Figs. 1, 2). Also many "blows", i.e., impulses, will be of insufficient strength to cause permanent surface deformations. However, many of these weaker blows will contribute to eventual surface fatigue failures. Such combined damage is shown in Figs. 2 and 3, the latter from the leading edge of a 400-series steel boiler feed pump blade. Figure 4 shows schematically the expected bubble pulse distribution from a cavitating venturi (4,5,7).

2. As surface roughness increases due to cavitation and/or corrosion effects, the flow pattern near the surface may be importantly altered. Also, accumulated cold-working of the material surface may affect, in either sense, its ability to resist further attack, i.e., increased strength and hardness will increase resistance, but increased brittleness will have the opposite effect. Thus the damage rate (volume loss rate

*NPSH is total (not static) head above "vapor head". NPSH is widely used in hydraulic machinery industry (2-5, eg.) to denote cavitation susceptibility of the liquid entering the machine (for pumps, eg.). ρ is liquid density.

per exposed area = MDPR*) in a given flow regime will not be constant with time, as emphasized by Thiruvengadam (13, 14, eg.). Figure 5 is a typical accumulated damage-time curve for either cavitation or liquid impact. There is typically an initial "incubation period", where little measurable loss occurs, presumably while fatigue processes proceed to the point necessary to cause surface failure. The damage rate then usually increases to a maximum, which may persist for some time, after which the rate decreases. Later secondary, tertiary and other maxima may occur in some cases. The later behavior depends primarily upon the interplay of flow-pattern alteration due to accumulated roughness, and material property changes due to accumulated permanent deformations and stressings (2-5, eg.).

B. More Speculative Observations and Conclusions

The detailed mechanisms whereby collapsing cavitation bubbles cause surface damage are not specified in the foregoing, since full agreement upon these detailed mechanisms does not yet exist. However, additional pertinent items to throw light on these detailed mechanisms are discussed next.

1. Typically, in normal cavitating flows, only one of 10^4-10^6 bubbles observed photographically to collapse near a surface actually cause a "crater", i.e., permanent deformation (15,16, eg.) even with easily deformable materials as soft aluminum. Such craters, (Figs. 1,2) judging from their spherical symmetry and unchanging contour with additional exposure (7,eg.) result from single bubble collapses. However, in carefully controlled flowing

*MDPR = mean depth of penetration rate = volume loss rate per exposed area. This is most common term for delineation of cavitation damage rate. See ASTM standard definition (12) for full explanation and related terms.

situations, as a venturi with spark-generated bubbles, a one-to-one correspondence between collapsing bubbles and observed craters can be attained if all parameters are correctly and precisely adjusted (17,18, eg.). Thus some very selective mechanism must delineate damaging from non-damaging collapses. The spherical collapse model of Rayleigh (6) provides only bubble diameter and wall distance as sorting parameters in a given flow regime. Intuitively these do not seem sufficient to justify such a large ratio ($\gtrsim 10^4$). However, if bubble collapse is highly asymmetric, as appears to be the actual case (17-25, eg.), an additional important sorting mechanism exists, i.e., "microjet" orientation with respect to the wall. Thus the very large ratio between non-damaging and damaging collapses is strong evidence for the predominence of asymmetrical collapses. This is confirmed photographically (17-22, 25, eg.) and by computer modelling (10,11,eg.).

2. The collapse of bubbles with approximate spherical symmetry through a sufficient radius ratio to generate damaging pressures (6,8,9,eg.) close enough to a wall to be damaging, i.e., essentially adjacent to the surface, and in real-flow situations involving pressure and velocity gradients, turbulence, etc., seems most unlikely. This statement is based on excellent photographs (17-22,25, eg.), as well as various analyses considering non-symmetrical boundary conditions (10,11,19-21, 23-26, eg.). Wall proximity, pressure gradients, gravity, and initial bubble

motion with respect to the liquid are all sufficient to drastically alter the collapse from approximate spherical symmetry to a toroidal mode, wherein the bubble is apparently pierced by a small "microjet" of liquid before its volume has been reduced by more than a factor of $\sim$10-100, i.e., diameter ratio < 5. Figure 6 from the author's laboratory (17,18, eg.) shows such bubble collapses in a venturi along a thin plate aligned parallel to the flow.

3. Theoretical analyses of bubble collapse assuming spherical symmetry but including real-fluid parameters of viscosity, surface tension, and compressibility (8,9, eg.) indicate that pressures around a collapsing bubble at the minimum possible wall distance (bubble initially contacting wall), if the bubble center were stationary during collapse, are not sufficient to explain the observed cratering for most materials. However, if the bubble "rebounds" from the minimum volume condition, as it would due to the compression of internal non-condensing gas or vapor, the calculated rebound pressures are such (8,9, eg.) that damage becomes much more likely. Such rebounds are made possible even in the absense of non-condensible gas, because the time period (few μs) is too short to allow full condensation even of the vapor. Also, theory (27, eg.) indicates that a collapsing bubble would migrate strongly toward a rigid surface and away from a free (or highly-resilient solid) surface (25,27,eg.). Only very few analyses (10,11,18,25,26, eg.) have investigated the effects of such bubble migration.

High-speed cinematography of collapsing bubbles in flowing or static regimes (17-22, 28-30, eg.) often show such rebounds, i.e., regrowth of the vapor mass, often several times, after traversing the minimum volume conditions, though usually not as spherical bubbles. Since entrained gas and non-condensed vapor at end of collapse are inevitable in most situations, such rebounds are to be expected. Further, in the toroidal collapse, mode, rebounds may be facilitated by the action of liquid vorticity.

4. Individual cavitation craters are often very similar to high-velocity, liquid impact craters. This is well demonstrated by comparing cavitation and droplet impact craters on plexiglass (Figs. 7 and 8, see refs. 4 and 5 for further detail). Both show the unusual response of plexiglass to liquid impact, i.e., an undamaged central region surrounded by a region of annular failure, since plexiglass is more resistant to compressive than to tensile stresses. The plexiglass results emphasize the role of "microjet" impact rather than shock wave imposition in cavitation attack, since droplet impact ($\sim$1 mm dia.) was in fact the mechanism of Fig. 8.

This conclusion is reinforced by Fig. 9 from venturi tests in the author's laboratory (4,5, eg.), showing cavitation pits upon cadmium-plated stainless steel. The cadmium is completely removed in the center of the pits, exposing the underlying stainless steel. This "washed" region is surrounded by a region where the cadmium is partially removed. This "washing" is presumably due to the very high liquid radial velocity generated by microjet impact shown schematically in Fig. 10. Photographic and theoretica

evidence (31-33, eg.) indicate that such radial velocities can be several times the original impact velocity, since they originate from a region of "water hammer" rather than steady-state stagnation pressure (3-5, 18, 31-33, eg.). It is clear that this damage pattern is not consistent with the classical Rayleigh liquid shock-wave model (6), but rather with the microjet impact model.

C. Conclusions from Foregoing Points

1. In many, if not most, engineering situations the mechanical portion of cavitation damage is due more to liquid microjet impact (Fig. 10) than to the imposition of spherical shock waves from the center of collapse, as supposed by Rayleigh (6).

2. Even if the bubble collapse is not approximately spherical, still the surrounding liquid pressure increases as the bubble volume is reduced. Intuitively, the pressure rise and collapse velocity will be reduced as the degree of spherical symmetry is reduced, but only limited quantitative data exists (10,11, eg.).

3. Thus while in the author's opinion the microjet impact mechanism is probably the most important in mechanical (non-corrosive) cavitation damage production, it is probable that the pressure rise around a rebounding bubble is also heavily involved. Schlieren and interferometric pictures confirm the presence of liquid shock waves around collapsing or growing bubbles (29,30, eg.).

4. Mechanical cavitation damage is the result of the highly transient imposition on the damaged surface of very intense and highly local forces ("blows"). These are associated with bubble

collapse rather than nucleation, since the damage occurs in the collapse region. Hence, modification of the flow geometry in the damaged region may not be effective in reducing damage since the bubbles are generated somewhere upstream.

5. Since cavitation loading is very transient and local in nature, surface coatings or treatments may be useful. In fact, very soft coatings such as rubber or elastomeric materials have often proven surprisingly resistant (34, eg.). This may be partially due to the effect of a resilient surface in repelling collapsing cavitation bubbles and orienting the resultant microjet away from the wall (18,25, eg.). Practical use of such coatings is, however, limited by the difficulty of maintaining a bond with the metallic wall (34, eg.).

The highly transient and local nature of cavitation attack provides also an important limitation in correlating cavitation damage resistance with conventional material mechanical properties since these are normally measured under quasi-static conditions and for relatively large sections. Thus they do not reflect accurately the loading conditions due to cavitation bubble collapse.

6. Mechanical cavitation damage results then primarily from a combination of liquid shock wave effects generated mostly during bubble "rebound" (Fig. 6) with the impact of a liquid microjet (Figs. 6 and 10). Essentially symmetric collapses are the exception, if not an impossibility, near solid surfaces or in regions of substantial pressure or velocity gradients, as almost inevitably will occur in most real flow situations. Local cavitation within the microjet(4,31,eg.) is also a possibilit

III. CAVITATION EROSION PREDICTION

A. General

Cavitation damage rates depend strongly of course upon material mechanical properties as well as upon flow and liquid parameters. However, no fully applicable relations yet exist. This is in general a highly complex (1-5, eg.) and difficult problem which is beyond the scope of the present article. However, a very brief review of presently available correlations will be given.

B. Mechanical Property Correlations

Figure 11 (35,36) summarizes this situation, taken from Heymann's discussion of ref. 35. A very comprehensive set of data, including both cavitation and liquid impact, from a material set ranging from very weak to very strong, was used. These studies (35,36) indicate that the best fit is obtained with ultimate resilence, $UR = (TS)^2/E$, where TS is tensile strength and E elastic modulus. However, the standard deviation is $\gtrsim 3$, and some materials may deviate by $\gtrsim 10$ from the best curve.

As explained in much more detail elsewhere (1-5, 35,36, eg.), it is desired to define a material mechanical property, $\mathcal{E}$ with units of energy per volume, representing the failure energy for the material under cavitation attack, such that the product $MDPR \cdot \mathcal{E}$ will be nearly constant over a broad range of material properties, but for fixed liquid flow parameters as velocity, pressure, temperature, geometry, etc. It is the general result of much research (1-5,35-39, eg.), that the best single mechanical property for a linear correlation is ultimate resilience, UR, representing essentially strain energy to failure if failure

is in the brittle mode. This expectation is consistent with numerous metallographic examinations of cavitation damage.

Traditionally, hardness has been used to correlate cavitation damage, and present results still confirm its utility for this purpose. As expected the correlation is not linear. Best fit results (39) show an exponent $n \cong 1.8$. This is roughly consistent with a linear UR fit, since hardness is approximately proportional to tensile strength. Therefore, a hardness exponent of 2 would be logically expected, rather than 1.8. However, in view of the general uncertainty of erosion data, this discrepancy is not significant.

Recommended correlating relations (4,5,eg.) based upon the above considerations are then

$$1/MDPR = C_1 \, UR \tag{1}$$

and

$$1/MDPR = C_2 \, BHN^{1.8} \tag{2}$$

where BHN is Brinell hardness. The correlating coefficient for the UR fit is somewhat the better (4,5,34, eg.) but not markedly so. The use of the BHN correlation is favored by the greater availability for most materials of hardness data as compared to ultimate resilience, and its greater ease of measurement.

The foregoing correlations apply of course only to the mechanical portion of cavitation or liquid impact damage, and thus entirely exclude corrosive effects. However, these are often very important, particularly in field machines where exposures are long, and the mechanical cavitation intensity is probably low compared to that encountered in the usual

"accelerated" laboratory devices. This situation, i.e., the inability to successfully model corrosive effects in laboratory cavitation test devices, appears to be a major reason for the present inability to predict cavitation damage effects in field devices from laboratory tests.

C. Methods for "a priori" Prediction of Onset and Rate of Cavitation Erosion

1. General

The prediction of the onset and extent of cavitation or liquid impact erosion can be attempted using theoretical and/or experimental techniques. However, one of the greatest problems today in the liquid erosion field is our present relative inability to predict erosion rates, or even their probable substantial eventual existance, in field machines from feasible laboratory tests or theoretical models. This is the case for all liquids of interest, ranging from ultra-low temperature cryogenic liquids to ultra-high temperature liquid metals. Even ratios of material resistance to that of a standard material measured in the same type of facility often differ widely between laboratories, as indicated in recent "round-robin" tests (40-42,eg.). This is particularly true for cavitation as opposed to liquid impact. As already mentioned, probably the primary difficulty in predicting field results from laboratory tests, particularly for cavitation, is the present inability to correctly model corrosive effects in these highly accelerated mechanical effect tests. If the tests were to be conducted in "real time", they would not "per se" represent a useful technique. Thus it is

necessary to accelerate mechanical and corrosive effects equally. While some preliminary attempts to accomplish this have been made (43-45, eg.), it appears generally beyond the present state of the art. One possible solution, proposed especially in this article, is to measure the mechanical attack component directly, either in laboratory or field device, in terms of the individual bubble collapse pulses imposed upon the damaged surface. Corrosive potentials in field and laboratory can also be measured easily, so that a proper magnification of each effect between laboratory and field can then be made.

2. Computer Modelling and High-Speed Photography

Computer modelling of both bubble collapse and droplet or jet impact, having many important technological applications (including cavitation "microjet" impact) has been quite extensive (8-11, 19,20,23,24,31-33,eg) to mention typical examples. This subject is treated in more detail elsewhere (4,5,eg.) and will not be discussed extensively here. However, along with high-speed photography applied to both bubble collapse and jet or droplet impact (17-25, eg.), computer modelling of the fluid-dynamic as well as material reaction (25,32,33,eg.), to mention a few typical references, are most important tools for understanding and eventually predicting these liquid erosion processes. However, the present state of the art is such that the gap between these basic research techniques and the eventual erosion occurring in field machines is as yet too great, in the author's opinion, for the meaningful application of these techniques to erosion prediction. As explained next more direct measuring techniques seem necessary.

3. Direct Measuring Techniques

a. General - It appears necessary to measure directly in cavitating laboratory devices some easily and quickly measurable parameters, which can then be correlated with measured damage rate. The same parameters can then be measured in a field or prototype device, and used for eventual damage prediction. The most promising parameters for this purpose are to be found in the overall field of acoustics and noise.

b. Noise-Damage Correlating Techniques - Cavitation noise has often been used as an easily detectable and measurable parameter for determining cavitation inception "sigma",* i.e., the onset of cavitation in a given flow device, and also for evaluating the possibility of damage (4,5,eg.). Since it is well-known that cavitation "noise" is essentially a "white" noise out to very high frequencies (4,5,eg.), it is common to filter electronically low-frequenices to reduce proportionately machinery and non-cavitating flow noise, and thus allow the detection of the cavitation signal in the high-frequency regime ($\sim$ 0.1 MHz). Such overall noise measurements have been correlated with measured erosion in various cavitation devices including centrifugal pumps (46,47, eg.) and venturis (48,49). These experiments have generally shown that damage rate and noise intensity are roughly proportional, both maximizing for the centrifugal pumps tested (46,47, eg.) near the "knee" of the head vs NPSH curve. However, it seems unlikely that such correlations with essentially overall noise can have very general applicability, since a given noise level could be produced either by a multitude of essentially non-damaging low-energy bubble collapses, or by

*See next page for footnote

a few highly energetic damaging ones.

It thus seems necessary to quantify the overall noise into individual bubble collapse pulse-height distributions applied to the damaged surface. Recent work in the author's laboratory (4,5, 50-54, eg.) and elsewhere (55-58, eg.), both in vibratory and flowing facilities (50-53) has attempted to develop these individual bubble pulse height techniques.

c. Pulse-Height Spectra and Erosion Efficiency - Bubble collapse pulse-height spectra have been measured here (50-54, eg.) in both vibratory and flowing (venturi) cavitation facilities, using micropressure-transducers of as high resonant frequency as possible ($\sim$0.1 MHz), which represents the approximate present state-of-the-art in this regard. Tests in the vibratory facility used both water and molten sodium (50-52, eg.) over a considerable temperature range, while cold water alone was used in the venturi tests. A high-pass electronic filter was used in all cases. This sufficed to suppress the 20 kHz horn frequency in the vibratory tests.

Figures 12 and 13 show the correlations obtained between "acoustic power"/^{AP} (defined in terms of the individual bubble pulse-height spectra) and "erosion power"/^{EP}. For a given test material, "erosion power", is proportional to MDPR. As previously discussed and shown by Eq. (1) and (2), the product of an energy-failure parameter, $\mathcal{E}$, and MDPR is/presumably constant for a given material. For the tests used for Figs. 12 and 13, the micro-transducer face was located symmetrically to the damage specimens with respec

*Cavitation "sigma", $\sigma = (p_\infty - p_v)/\rho V_\infty^2/2$ sometimes called "cavitat number", signifies the likelihood and extent of cavitation in a gi flow regime. p_∞ and V_∞ are upstream pressure and velocity, and p_v is liquid vapor pressure.

to the cavitating field.

Figure 13 shows a linear relationship between venturi measured MDPR, proportional to "erosion power" for the soft aluminum (1100-0) test speimens, and "acoustic power" (or "spectrum area"), deduced from the measured bubble collapse height spectra (explained later). There is a small negative acoustic energy threshold. As shown in the schematic representation (Fig. 4), a positive bubble energy threshold would be expected. This discrepancy is probably due to the lack of sufficient sensitivity in the present instrumentation for the soft aluminum tests. Figure 12 shows that linearity did not hold over the full range of the vibratory tests, which include both water and sodium. Test material was 316 stainless steel over a greater range of acoustic power than in the venturi tests. These vibratory stainless steel results are best represented by an exponential relation (Eq. 3), where $n \cong 5$, and C is a constant of proportionality depending upon test facility parameters,

$$\text{MDPR} = C\ (\text{acoustic power})^{1/n} \qquad (3)$$

For the water venturi tests upon soft aluminum, $n \cong 1$, since results were linear. It will be useful to observe whether or not this linearity persists in the venturi for harder materials.

2. Acoustic Power From Pulse-Height Spectra

The normalized mean square value of the sound pressure, which is proportional to "acoustic power", is generally defined (49, eg.) as the "noise intensity", I, (Eq. 4).

$$I = p^2 / \rho C^2 \qquad (4)$$

where C is sonic velocity in the liquid and ρ is liquid density.

A classical treatment of acoustic power from a point source (27,53, eg.), using the linear approximation, shows the following.

$$W(R) = [(\text{area}/\rho C]\int_{t(R)}^{T(R)} p^2 \, dt \qquad (5)$$

where W(R) is the acoustic power radiated into the fluid at a distance R from the source. The pressure-squared relationships are to be expected for energy stored in an elastic medium, since displacement itself is then proportional to pressure.

For the present tests, pulse heights are of very short duration (few μs), and cover a very small surface area (~0.1 mm dia),as estimated from high-speed cinematography results (17,18, eg.). These are measured by micro-transducer (~4 mm dia. having resonant frequency of ~ 0.1 MHz. Hence the precision of the pulse shape measurements is necessarily limited. Thus a simplified square pulse shape (2 μs duration) was assumed. The resulting oscillograms were reduced "manually", due to the lack at that time of suitable multichannel-analyzer and pulse-shaper circuitry.

The oscillograms then provide directly data for pulse height spectra, PHS (Fig. 14). These are then converted to differential PHS (Fig. 15). Integral distributions, $N(p) = \int_p^\infty N(p)dp$ are then converted to distributions in p^2, i.e.

$$N(p^2) = \int_p^\infty N(p^2)dp.$$

Figure 16 is a typical example. The areas under these p^2 curves are then proportional to PHS acoustic power,computed in conventional units as watts. The low pressure portion of

Fig. 16 is completed as a horizontal line. Data was not received in this area, since the instrumentation was "saturated" by the large number of low intensity "blows". Since it is presumed that only relatively high-energy pulses contribute to damage (Fig. 4), this approximation is hopefully not important for damage correlations such as Figs. 12 and 13.

Figure 15 shows maximum transducer pulse pressures of only 600 psi ($\sim$41 bar), which would obviously not be damaging even to the 1100-0 aluminum test material. However, actual pressures were no doubt much greater because of the lack of both spacial and temporal distribution of the micro-transducer used, as already discussed. By far the largest part of this discrepancy appears due to the spatial problem, i.e., the large ratio between the microprobe active area ($\sim$3 mm dia.) and that of the impacting cavitation microjet, of which the probable diameter is $\sim$1-10 μm (17,18,eg.). Thus the probable area ratio is probably $\sim 10^6$, so that the measured pressure pulse amplitudes ($\sim$40 bar) appear to indicate extremely high actual local surface pressures. Other more precise measurements (59, eg.), indicate bubble collapse pressures of $\sim 10^4$ bar, obviously adequate to create individual craters in almost any test material, even hardened steels or Stellites.

3. Cavitation Erosion Efficiency

The ratio of "erosion power" (MDPR$\cdot\mathcal{E}$, where $\mathcal{E}$ = ultimate resilience for present purposes) and "acoustic power" has been defined (4,5,50-54,eg.) as cavitation erosion efficiency η_{cav}, i.e.,

$$\eta_{cav} = \text{(erosion power)/(acoustic power)} \qquad (6)$$

Presently available measurements of η_{cav} (4,5,50-54, eg.) indicate

it to range between $\sim 10^{-8}$ and 10^{-6}. The higher values were measured in the soft aluminum venturi tests discussed above, and the lower values from previous vibratory facility tests upon more resistent materials (50-52, eg.). The standard deviation for all these measurements has been $\lesssim 20\%$, which is about typical for most liquid erosion tests.

While the pressure-pulse spectrum technique here described has so far only been applied to non-rotating components, it appears also pertinent to rotating ones, although obvious geometrical difficulties need be considered. It thus appears possible that an "a priori" damage predicting capability may become available in the relatively near future using such a technique for a variety of fluid-flow machines.

d. Erosion and Acoustic-Emission Noise

Acoustic-emission noise from cavitation-induced material deformation (microcrack formation, etc.) is a well-known phenomenon which could conceivably be used to measure "in situ" cavitation erosion as it occurred. It has been applied already to non-cavitating liquid erosion (60). However, it seems unlikely that this technique can be adapted successfully to the cavitating case (4,5,60,eg.), since cavitation noise itself is an order of magnitude greater than that expected from acoustic emission. Also they appear to cover similar frequency ranges. This negative expectation may prove erroneous, since no pertinent tests have as yet been made.

Pertinent to this possibility is the observation here from venturi high-speed cinematography (17) of an apparent ejected cavitation debris particle from soft aluminum. Ejection velocity normal to the material surface was ~100 m/s. The particle was of elongated shape (~1 mm length). If such high ejection energy is typical, the associated noise might prove easily detectable.

e. Cavitation Debris Tracer Techniques

Tests were conducted here in a venturi loop (4,5,61) using neutron-irradiated stainless steel specimens both in cavitating water and mercury. The debris was sorted by filter-bank, and the quantities determined by radiation counting techniques. Particle diameters to ~1 mm were found, with the greatest number much smaller (4,5,61). Obviously this technique is generally restricted to closed-loop situations. However, somewhat similar tests using irradiated paint in a water turbine situation have been reported (62) to determine the existence of damaging cavitation rather than quantitative damage measurements.

f. Characteristic Erosion Curve for Damage Prediction

It is sometimes assumed that the characteristic S-shaped erosion-time curve (Fig. 17) is actually a "universal erosion curve", i.e., the same shape applies, except for scale factors, for all materials and tests. The measurement of the early portion of this curve could then be used to predict the remainder. The overall question of the detailed shape of erosion-time curves is highly complex (1-5,13,14,eg.) and generally not

within the scope of this article. However, the assumption of a "universal" damage curve, including together both cavitation and liquid impact damage (1-5,63-66,eg.) is perhaps defensible for approximate damage prediction, since other more precise methods are presently lacking.

The procedure would then be to measure the entire damage-time curve for a "soft" material and also for the candidate material, using whatever laboratory device is available. The "incubation period" (Fig. 5) would then be measured in a prototype or field machine on soft material inserts which had been tested in the laboratory, or upon an easily erodable coating (67, eg.), which also could be tested in the laboratory. The laboratory tests could then be used to establish a ratio between resistances of the "soft" material and the candidate prototype material. From the resulting data, the erosion history of the prototype machine could be estimated.

While these ideas have been discussed for some time (1-5, 35, eg.), more recent work has attempted to develop a relation between incubation period, IP and $MDPR_{max}$ as Eq. (7).

$$IP^n = C_1/MDPR_{max} \tag{7}$$

where C_1 depends upon material properties, details of the test facility, test liquid parameters, etc. For a given material and type of test, C_1 should remain constant. Available estimates of n (63-66, eg.), from both cavitation and liquid impact data, indicate $0.6 \lesssim n \lesssim 1.0$. Hence, it appears that this is far from an accurate predicting technique at this time, and an entirely

"universal" damage-time curve is not a reality. Still, in the lack of more precise erosion predicting methods, this technique has a certain utility.

IV. CONCLUSIONS

Certain important conclusions can be drawn from the material reported in this article.

1) In the present state of the art, the full and detailed mechanisms producing cavitation damage are not entirely known or agreed in spite of more than half a century of research (1-5, eg). However, certain basic, agreed-upon principles exist and are here listed. Other more tentative conclusions based both upon experimental observations and computer modelling have also been discussed.

2) A broad divergence still exists between the maximum possibilities of computer modelling and the prediction of cavitation erosion as it occurs in the field. This gap is found both in the realms of bubble dynamics and material reaction. A full discussion of these questions is beyond the scope of this article. However, it is not yet possible, or likely to be in the near future, to predict cavitation erosion rates, or even their existence in prototype or field machine from given conventional flow parameters. It is, therefore, necessary to consider and develop other more "empirical" predicting methods. This is a major subject of the present article.

3) The simplest and most promising of such predicting methods are those based upon acoustic techniques. It has already been shown that at least for certain special cases,

there is a reasonably linear correlation between erosion rate and overall noise intensity (46-49, eg.). However, the generality and applicability of this method is limited, because a given sound intensity can be due either to very numerous low-energy non-damaging pressure pulses, or a few of very high energy and damaging capabilities. To obviate this difficulty, a new technique, using individual bubble collapse pulse-height analyses to correlate damage, has been developed here (50-54, eg) and elsewhere (55-58, eg.).

4) The ratio of "erosion power" and acoustic power as computed from the pulse-height spectra (50-54, eg.), has been here defined as "cavitation erosion efficiency, η_{cav} (4,5,50-54, eg.). Measured η_{cav} values ($\sim 10^{8}$-10^{6}) depend upon numerous test parameters. However, these large ratios are consistent with theoretical expectations, being primarily due directly to the large area ratio ($\sim 10^{6}$) between microprobe sensitive area and impinging cavitation "microjet" area (17,18, eg.). Also involved in the discrepancy are the limited spatial and temporal (~ 1 μs required) response capabilities of the microprobe, and probably less important, "acoustic impedance ratio" between liquid and damaged material, affecting the ratio between absorbed and reflected energy.

5) Other "in situ" direct measurement techniques of apparently relatively limited applicability are the use of material "acoustic emission" and debris collection using irradiated damage specimens (61-62, eg.).

6) A hypothetical assumed "universal" damage-time curve (Fig. 5) for both cavitation and liquid impact erosion can be

used (1-5, 35, 63-66 , eg.) to estimate eventual erosion performance of prototype or field machines, comparing tests results upon a special "soft" material and a candidate material in laboratory test devices, with performance of "soft" damage inserts in the actual machine. This technique is cumbersome and expensive, and available results show that predictions are highly uncertain. However, it has a certain utility in the absence of other more precise techniques.

7) Best available correlations between conventional material mechanical properties are most successful using either ultimate resilience ($UR = TS^2/2E$) or Brinell hardness, BHN (Eqs. 1 and 2). However, the standard deviations are $\gtrsim 3$, and the discrepancy for certain materials $\gtrsim 10$. Hence, the engineering value of such correlations for previously untested materials is limited. The correlation with inverse MDPR (mean depth of penetration rate) is linear with UR, but proportional to $BHN^{1.8}$. These correlations would be consistent, as well as dimensionally-consistent, if BHN^2 were used, since $BHN \propto TS$. This relatively minor discrepancy is not believed important considering the generally inconsistent nature of all liquid erosion results.

8. The greatest difficulty (1-5, eg.) in predicting field results from laboratory tests is probably due to the inability to model corrosive effects in mechanically-accelerated laboratory tests.

Bibliography

1. A. Thiruvengadam, "Cavitation Erosion," Appl. Mech. Rev., ASME, vol. 24, no. 3, March 1971, pp. 245-253.

2. R. T. Knapp, J. T. Daily and F. G. Hammitt, Cavitation, McGraw-Hill, N.Y., 1970.

3. F. G. Hammitt and F. J. Heymann, "Liquid-Erosion Failures" in Metal Handbook, vol. 10, ed. 8, pp. 160,167, Amer. Soc. of Metals, Metals Park, Ohio, 1975.

4. F. G. Hammitt, Cavitation and Multiphase Flow - Theory and Practice, McGraw-Hill, N.Y., 1979.

5. F. G. Hammitt, "Cavitation and Liquid Impact Erosion," Chap. 11, Wear Control Handbook, ASME (1980), edit. M. B. Peterson.

6. Lord Rayleigh, "On the Pressure Developed in a Liquid During the Collapse of a Spherical Cavity," Phil. Mag, v. 34, pp. 94-98, 1917.

7. F. G. Hammitt, et al, "Initial Phases of Damage to Test Specimens in a Cavitating Venturi," Trans. ASME, J. Basic Engr., v. 87, ser. D, no. 3, pp. 347-359, 1963.

8. R. Hickling and M. S. Plesset, "Collapse and Rebound of a Spherical Bubble in Water," The Physics of Fluids, vol. 7, no. 1,pp. 7,14, 1964.

9. R. D. Ivany and F. G. Hammitt, "Cavitation Bubble Collapse in Viscous, Compressible Liquids Numerical Analysis," Trans. ASME, J. Basic Engr., vol. 87, ser. D, no. 5, pp. 977, 985, 1965.

10. M. S. Plesset and R. B. Chapman, "Collapse of an Initially Spherical Vapor Cavity in the Neighborhood of a Solid Boundary," J. Fluid Mech., vol. 47, no. 2, p. 283, May 1971.

11. T. M. Mitchell and F. G. Hammitt, "Asymmetric Cavitation Bubble Collapse," Trans. ASME, J. Fluid Engr., vol. 95, no. 1, pp. 29-37, March, 1973.

12. ASTM Committee G-2, Standard Definitions of Terms Relating to Erosion by Cavitation and Impingement," 1973, ASTM, Phila.

13. A. Thiruvengadam, "A Unified Theory of Cavitation Damage," Trans. ASME, J. Basic Engr., vol. 85, ser. D, no. 3, pp. 365,376, 1963.

14. A. Thiruvengadam, "Effects of Hydrodynamic Parameters on Cavitation Erosion Intensity," Hydronautics Tech. Rept. 233-14, Nov. 1970.

15. M. J. Robinson and F. G. Hammitt, "Detailed Damage Characteristics in a Cavitating Venturi," Trans. ASME, J. Basic Engr., v. 89, ser. D, no. 1, pp. 161-173, 1967.

16. R. T. Knapp, "Recent Investigations of the Mechanics of Cavitation and Cavitation Damage," Trans. ASME, pp. 1045-1054, Oct. 1955.

17. C. L. Kling, "A High-Speed Photographic Study of Cavitation Bubble Collapse," Ph.D. thesis, Nuclear Engr. Dept., University of Michigan, 1979; also available as Univ. of Mich. ORA Rept. UMICH 03371-2-T, March, 1979.

18. E. E. Timm, "An Experimental Photographic Study of Vapor Bubble Collapse and Liquid Jet Impingement," Ph.D. thesis, Chem. Engr. Dept., University of Michigan, 1974; also available as Univ. of Mich. ORA Rept. UMICH 01357-39-T, June, 1974.

19. C. G. Naude and A. T. Ellis, "On the Mechanism of Cavitation Dama by Nonhemispherical Cavities Collapsing in Contact with a Solid Boundary," Trans. ASME, J. Basic Engr., v. 83, ser. D, no. 4, pp. 648-656, 1961.

20. T. B. Benjamin and A. T. Ellis, "The Collapse of Cavitation Bubbl and the Pressures Thereby Produced Against Solid Boundaries," Phi Trans. Roy. Soc., ser. A, v. 260, no. 1110, pp. 221-240, 1966.

21. N. D. Shutler and R. B. Mesler, "A Photographic Study of the Dyna and Damage Capabilities of Bubbles Collapsing Near Solid Boundari Trans. ASME, J. Basic Engr., v. 87, ser. D, no. 2, pp. 511-517, 1

22. R. D. Ivany, F. G. Hammitt, and T. M. Mitchell, "Cavitation Bubbl Observations in a Venturi," Trans. ASME, J. Basic Engr., v. 88, ser. D, no. 3, pp. 649-657, 1966.

23. A. Eller and H. G. Flynn, "The Equilibrium and Stability of a Translating Cavity in a Fluid," J. Fluid Mech., v. 30, pt. 4, pp. 785-803, 1967.

24. H. C. Yeh and W. J. Yang, "Dynamics of Bubbles Moving in Liquids with Pressure Gradient," J. Appl. Phys., vol. 19, no. 7, pp. 3156 3165, 1968.

25. D. C. Gibson, "The Collapse of Vapor Cavities," Ph.D. thesis, Churchill College, Cambridge University, July, 1967.

26. A. N. Korovkin and Y. L. Levkovskiy, "Closing of Cavitation Caver Close to a Solid Wall," (in Russian), J. of Engr. Phys., vol. XII, no. 2, pp. 246-253, April, 1967.

27. R. H. Cole, Underwater Explosions, Dover Publ. Inc., 1965.

28. R. T. Knapp and A. Hollander, "Laboratory Investigations of the Mechanism of Cavitation," Trans. ASME, 70, pp. 419-435, 1948.

29. A. T. Ellis, "On Jets and Shock Waves from Cavitation," Proc. 6th Naval Symp., Oct. 1966, pp. 6-1 to 6-19, Washington, D.C.

30. W. Lauterborn and H. Bolle, "Experimental Investigations of Cavit Bubble Collapse in the Neighbourhood of a Solid Boundary," J. Flu Mech., vol. 72, no. 2, pp. 391-399, 1975.

31. Y. C. Huang, "Numerical Studies of Unsteady, Two-Dimensional Liqu Impact Phenomena," Ph.D. thesis, Mech. Engr. Dept., Univ. of Mich also available as U-M ORA Rept. UMICH 03371-8-T, June, 1971; see Y. C. Huang, F. G. Hammitt, and W. J. Yang, "Hydrodynamic Phenome During High-Speed Collision Between Liquid Droplet and Rigid Plar Trans. ASME, J. Fluids Engr., v. 95, ser. D, no. 2, pp. 276,294,

32. J. B. Hwang, "The Impact Between a Liquid Drop and an Elastic Hal Space," Ph.D. thesis, Mech. Engr. Dept., University of Michigan; also available as U-M ORA Rept.UMICH 012449-5-T, March, 1975.

33. J. B. Hwang and F. G. Hammitt, "Transient Distribution of the Stress During the Impact Between a Liquid Drop and an Aluminum Body," BHRA 3rd Int'l Symp. Jet Cutting Technology, May 11-13, 1976, Chicago; also as U-M ORA Rept. UMICH 012449-8-T, June, 1975.

34. J. Z. Lichtman, D. H. Kallas, C. K. Chatten, and E. P. Cochran, Jr., "Cavitation Erosion of Structural Materials and Coatings," Corrosion, 497t-505t, Oct. 1961.

35. F. G. Hammitt, Y. C. Huang, et al, "A Statistically Verified Model for Correlating Volume Loss Due to Cavitation or Liquid Impingement," ASTM STP 474, pp. 288-322, 1969.

36. F. J. Heymann, Discussion of Ref. 35, ASTM STP 474, pp. 312, 1969.

37. B. C. Syamala Rao, N. S. Lakshama Rao and K. Seetharamiah, "Cavitation Erosion Studies with Venturi and Rotating Disk in Water," Trans. ASME, J. Basic Engr., vol. 92, pp. 563,579, Sept. 1970.

38. F. J. Heymann, "Toward Quantitative Prediction of Liquid Impact Erosion," ASTM STP 474, pp. 212, 248, 1969.

39. F. J. Heymann, "Erosion by Cavitation Liquid Impingement and Solid Impingement," Westinghouse Electric Engr. Rept. E-1460, June, 1968.

40. F. G. Hammitt, C. Chao, C. L. Kling and D. O. Rogers, "ASTM Round-Robin Test with Vibratory Cavitation and Liquid Impact Facilities of 6061-T-6511 Aluminum Alloy, 136 Stainless Steel, Commerically Pure Nickel, ASTM Materials Research and Standards, MTRSA, v. 10, no. 10, pp. 16,36, 1970.

41. F. J. Heymann, "Preliminary Report on Liquid Impact Erosion, Round-Robin Test Program," Westinghouse Steam Turbine Division, Internal Rept., July 1973.

42. ASTM Standards, Standard Method of Vibratory Cavitation Erosion Test, ANSI/ASTM G32-77, 1977.

43. S. Nemecek, Kotazce urcovani kavitacni odolnosti, Konference o vodnich turbinach, 1958, Brno.

44. S. Nemecek, Kotazce mechaniky kavitace, I. shornik praci Vysoke skoly strojni v Liberci, pp. 128-146, 1959.

45. K. Steller, Personal communications with F. G. Hammitt, Inst. Fluid Flow Mach., Polish Aca. Science, Gdansk, Poland, 1976.

46. I. S. Pearsall and P. J. McNulty, "Comparisons of Cavitation Noise with Erosion," 1968 ASME Cavitation Forum, pp. 6,7.

47. J. J. Varga and Gy. Sebestyen, "Determination of Hydrodynamic Cavitation Intensity by Noise Measurement," Proc. Second Int'l JSME on Fluid Machinery and Fluidics, Sept. 1972, pp. 285-292, Tokyo; see also J.J. Varga, Gy. Sebestyen and A. Fay, "Detection of Cavitation by Acoustic and Vibration-Measurement Methods," La Houille Blanche, no. 2, pp. 137,149, 1969.

48. P. A. Lush and S.P. Hutton, "The Relation Between Cavitation Intensity and Noise in a Venturi-Type Section," Proc. Int'l Conf. on Pump and Turbines, Sept. 1976, pp. 1,3, NEL, Glasgow, Scotland.

49. A. S. Ramamurthy and P. Bhaskaran, "Velocity Exponent for Erosion and Noise Due to Cavitation," Trans. ASME, J. Fluids Engr., March 1979, v. 101, pp. 69-75.

50. F. G. Hammitt and J. B. Hwang, "Ultrasonic Cavitation Regime Pulse-Count Spectra as Related to Cavitation Erosion," Proc. Seventh Int'l Non-Linear Acoustics Conf., Aug. 1978, Blacksburg, Va.

51. F. G. Hammitt, S. A. Barber, M. K. De and A. N. El Hasrouni, "Predictive Capability for Cavitation Damage from Bubble Collapse Pulse Count Spectra," Proc. Conf. Scaling for Performance Predict in Rotodynamic Machines, Inst. Mech. Engrs., 6-8 Sept., 1977, University of Stirling, Scotland.

52. F. G. Hammitt, S. A. Barber, M. K. De and A. N. El Hasrouni, "Cavitation Damage Prediction from Bubble Collapse Pulse Count Spectra," 1977, ASME Cavitation and Polyphase Flow Forum, pp. 25-28, 1977.

53. F. G. Hammitt and M. K. De, "Cavitation Erosion of Aluminum Considering Bubble Collapse Pulse Height Spectra and Cavitation Erosion Efficiency," Proc. 1979 Intl. Wear Conf., ASME, Dearborn, April, 1979; Rept. No. DRDA UMICH 014456-33-I, Aug. 1978, Univers of Michigan, Ann Arbor, Michigan.

54. F. G. Hammitt, M. K. De, J. Elenz, E. Hunt, "Venturi Cavitation Bubble Collapse Pulse Spectra and Observed Pits in Soft Aluminum, 1978 ASME Cavitation and Multiphase Flow Forum, June 1978, 31-33.

55. F. Numachi, "An Experimental Study of Accelerated Cavitation Induced by Ultrasonics," Trans. ASME, J. Basic Engr., vol. 87, pp. 967-976, 1965.

56. F. Numachi and M. Hongo, "Ultrasonic Shock Waves Emitted by Cavitation Erosion Spectra Analysis of Pulse-Heights Producted by Cavitation Bubbles," Proc. Sixth Non-Linear Acoustics Conf., July 1975, Moscow (Odessa Poly. Inst.).

57. V. K. Makarov, A. A. Kortnev, S. G. Suprun, and G. I. Okolelov, "Cavitation Erosion Spectra Analysis of Pulse-Heights Produced by Cavitation Bubbles," Proc. Sixth Non-Linear Acoustics Conf., July 1975, Moscow (Odessa Poly. Inst.).

58. F. Numachi, "Transitional Phenomena in Ultrasonic Shock Waves Emitted by Cavitation on Nydrofoils," Trans. ASME, J. Basic Engr. vol. 81, p. 153, June, 1959.

59. G. W. Sutton, "A Photo-Elastic Study of Strain Waves Caused by Cavitation," J. Appl. Mech., vol. 24, no. 3, pp. 340, 38, 1957.

60. Personal communication, J. R. Frederick, Univ. of Mich, 1978.

61. W. J. Walsh and F. G. Hammitt, "Cavitation and Erosion Damage Measurements with Radio-Isotopes," Nuc. Sci. and Engr., vol. 14, no. 3, pp. 217-223, Nov. 1962.

62. S. L. Kerr and K. Rosenberg, "An Index of Cavitation Erosion by Means of Radioisotopes," Trans. ASME, v. 80,1958, 1308-1314.

63. F. G. Hammitt, "Damage to Solids Caused by Cavitation," Phil. Trans. Roy. Soc., ser. A, vol. 260, no. 1110, pp. 245,1966.

64. G. S. Springer, Erosion by Liquid Impact, Scripta Publ. Co., 1976, Washington, D.C.

65. Gy. Sebestyen, F. Sturteczby, A. Szabo, "Some Results of Cavitation Erosion Investigations in a Pump," Proc. 3rd Conf. on Fluid Mechanics and Fluid Machinery, Akademiai Kiado, Budapest, 567-574, 1969.

66. J. J. Varga, I. Bata, Gy. Sebestyen, "Investigations on Cavitation Erosion in Rotary Disc Equipment and Some Results," ibid no. 156, p. 694-704, 1969.

67. R. S. Kulp and J. V. Altieri, "Cavitation Damage of Mechanical Pump Impellers Operating in Liquid Metal Space Power Loops," NASA CR-165 (prepared Pratt and Whitney Aircraft Div.), July, 1965.

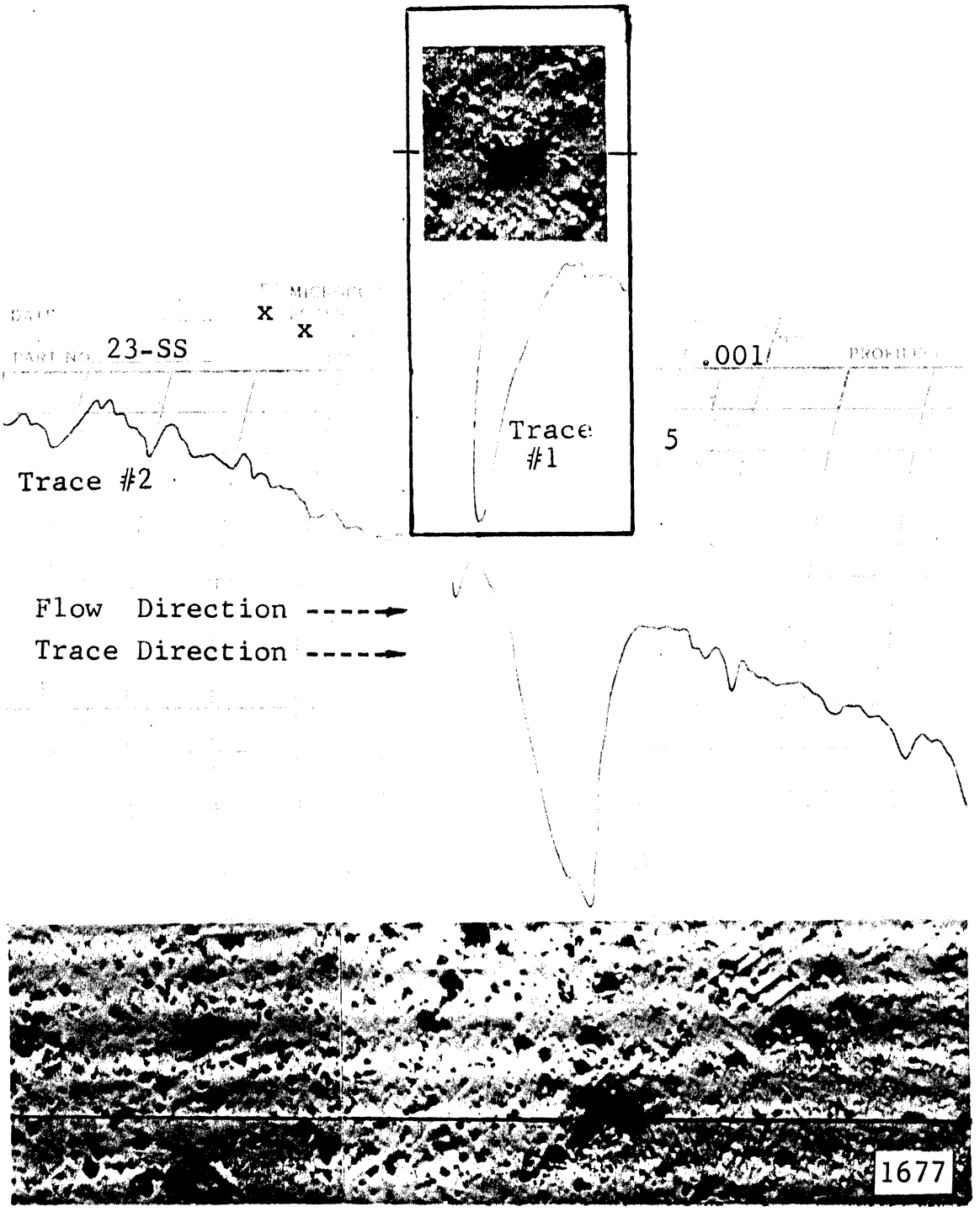

Figure 1. Photomicrograph and corresponding proficorder traces of surface of specimen 23-SS (type 304 stainless steel), after 10 hours exposure to "standard cavitation" in mercury at a throat velocity of 34 ft. per sec. (#1677)

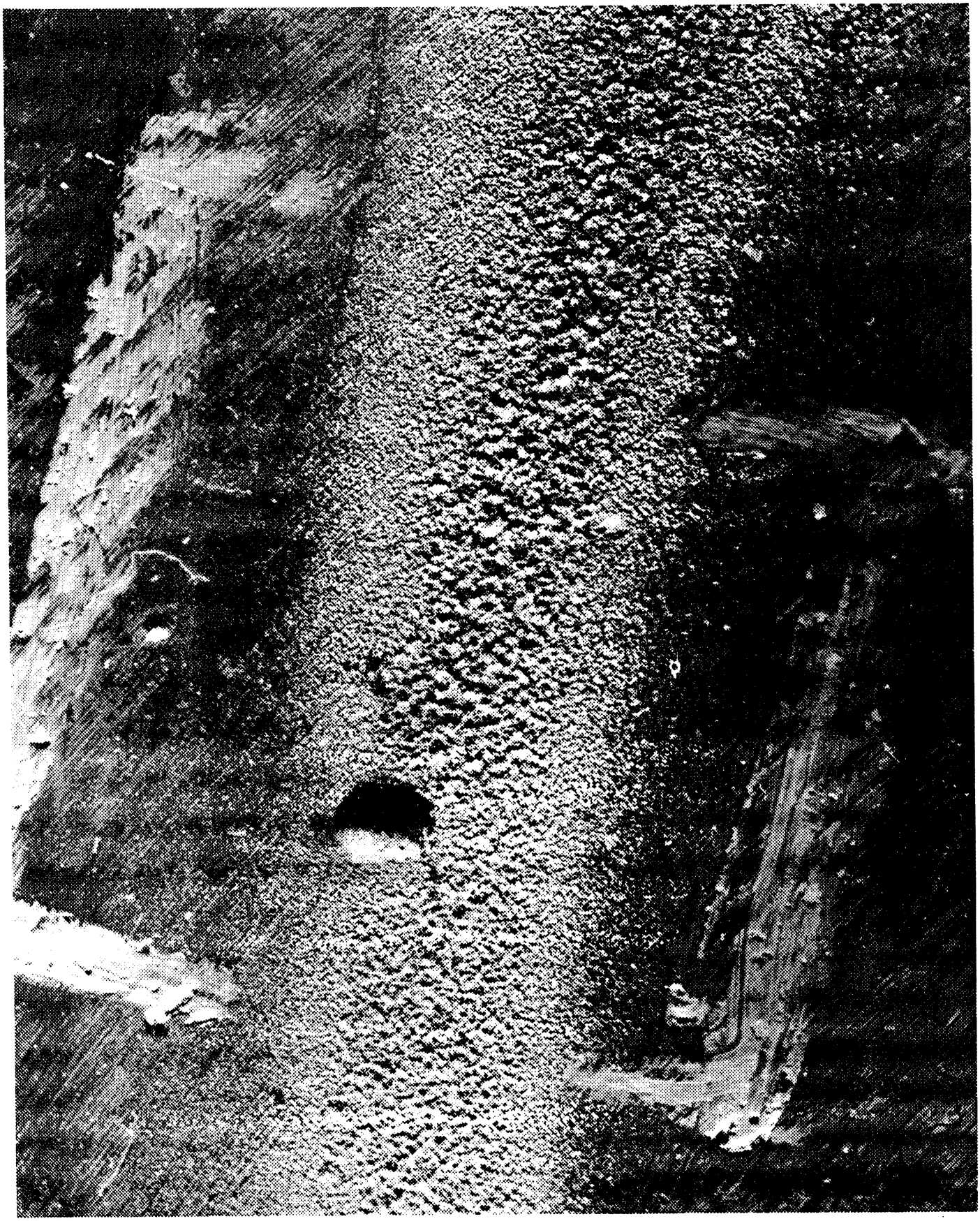

Figure 2. Cavitation Damage on shroud of mercury centrifugal pump. University of Michigan mercury tunnel. Larger crater diameter = 3 mils. (#1185)

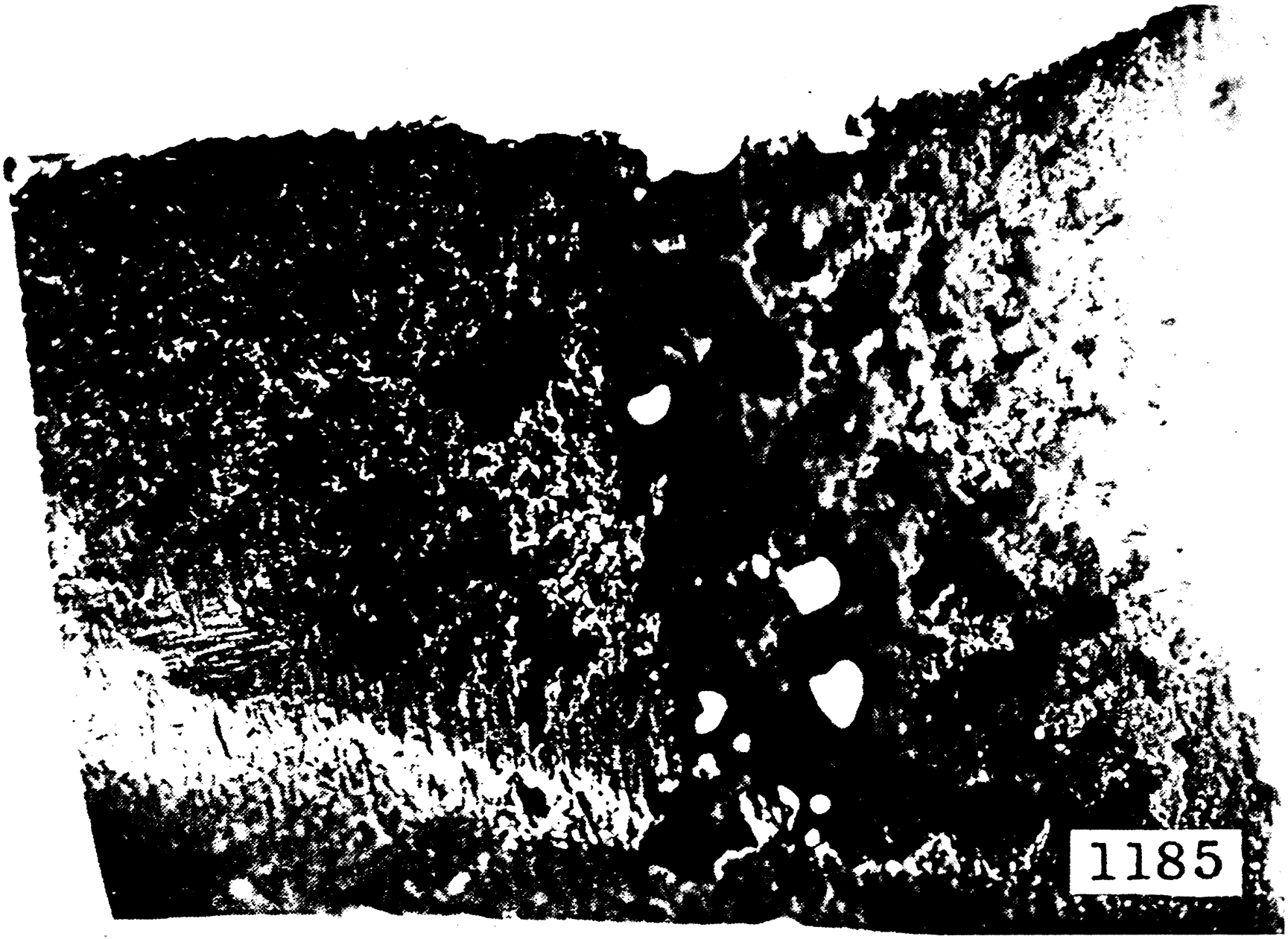

Figure 3. Leading edge of a series 400 stainless steel impeller for a boiler feed pump, exhibiting deep local damage caused by cavitation erosion. (#1185)

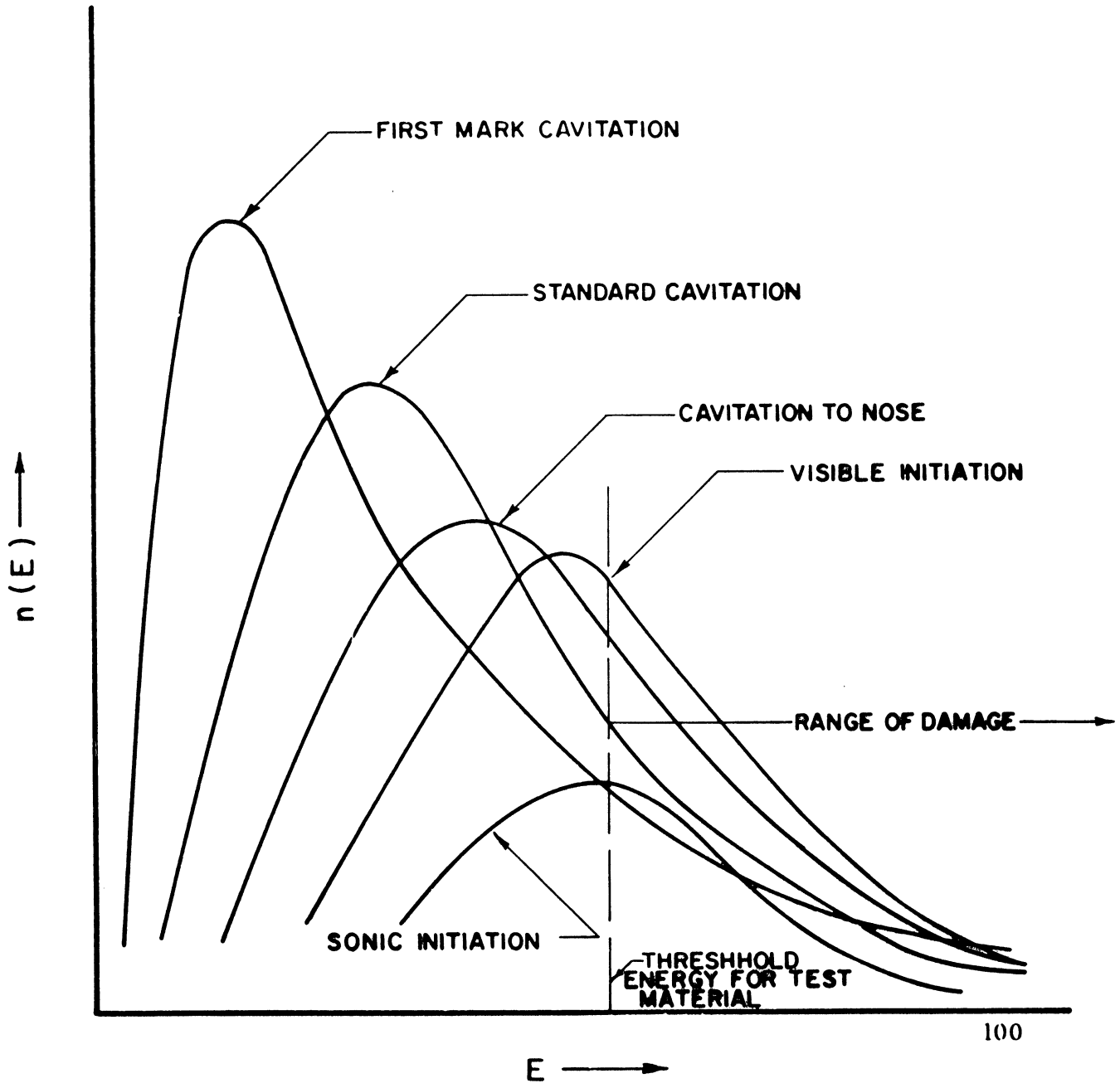

Figure 4. Hypothesized bubble energy spectra for various cavitation conditions at a constant velocity, for a given material in U-M venturi. (#100)

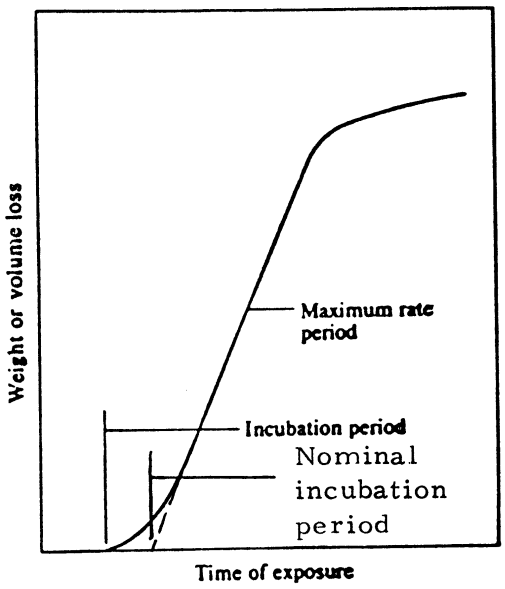

Figure 5. Typical Cavitation or Liquid Impact "S-Shaped) Erosion Curve.

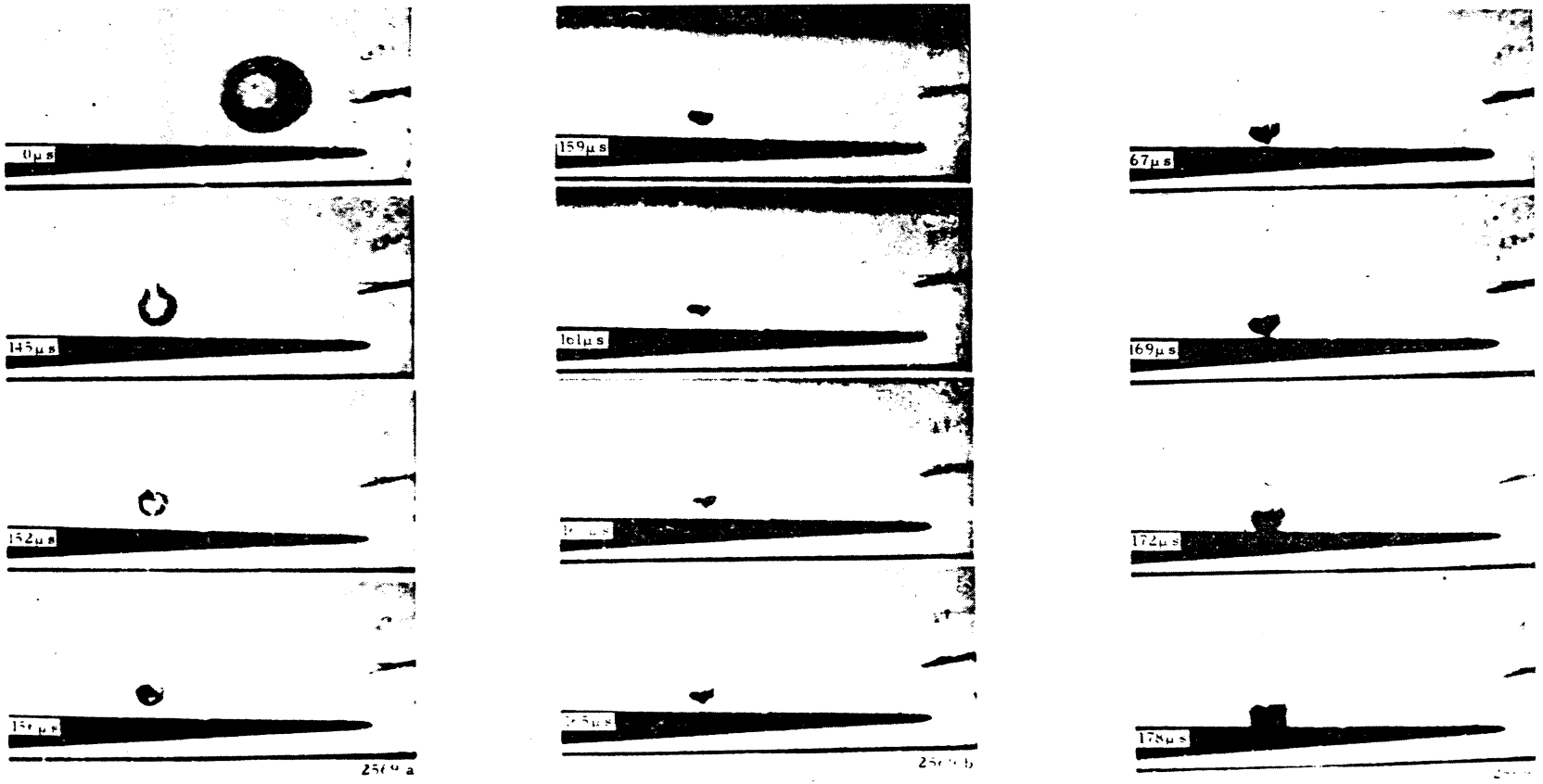

Figure 6. Bubble collapsing along plate in water venturi. Flow is right to left, and bubble is created by spark electrode shown. (#2569)

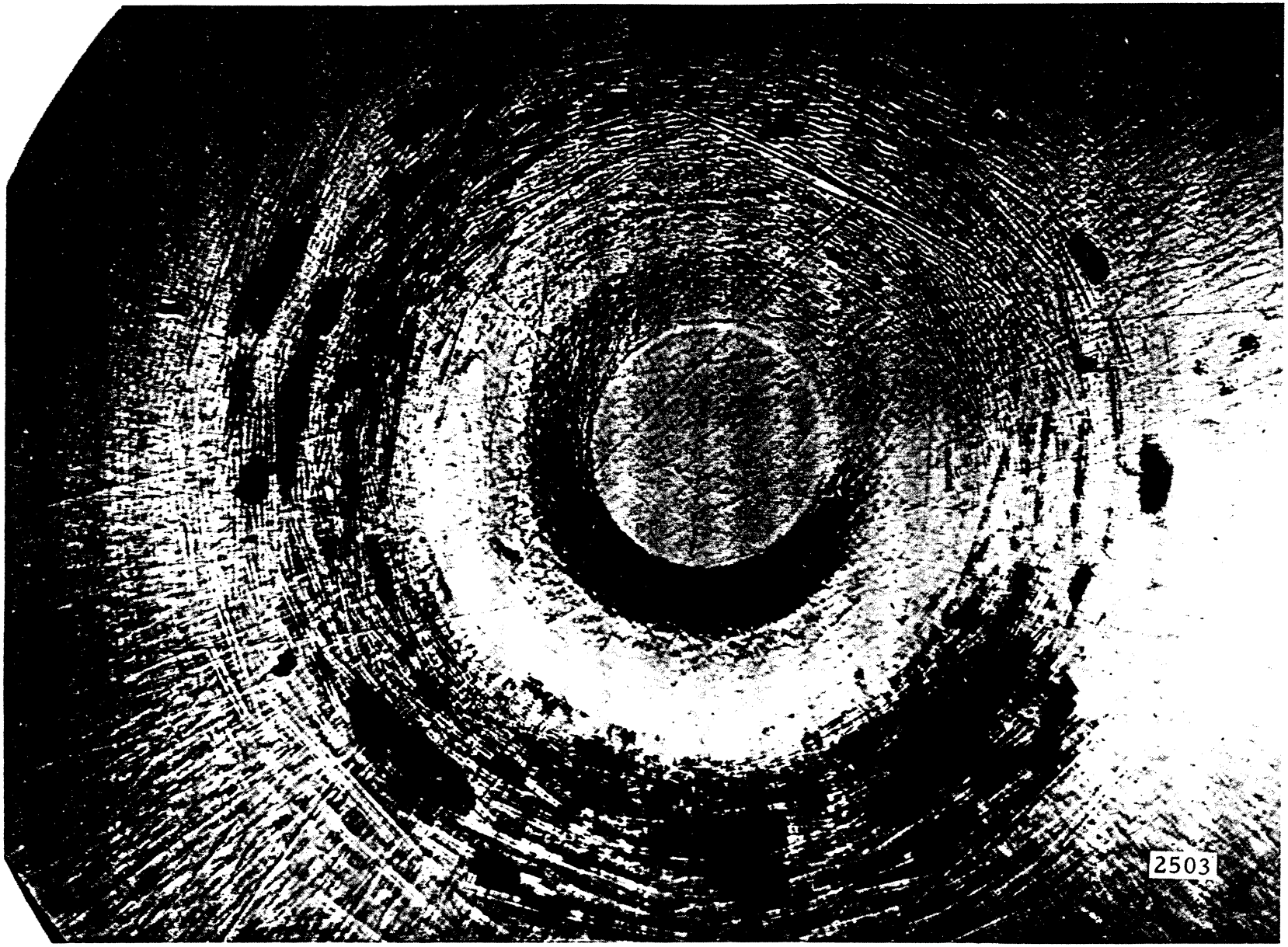

Figure 7. Damage produced on a plexiglass surface by the impingement of liquid jet. (#2503)

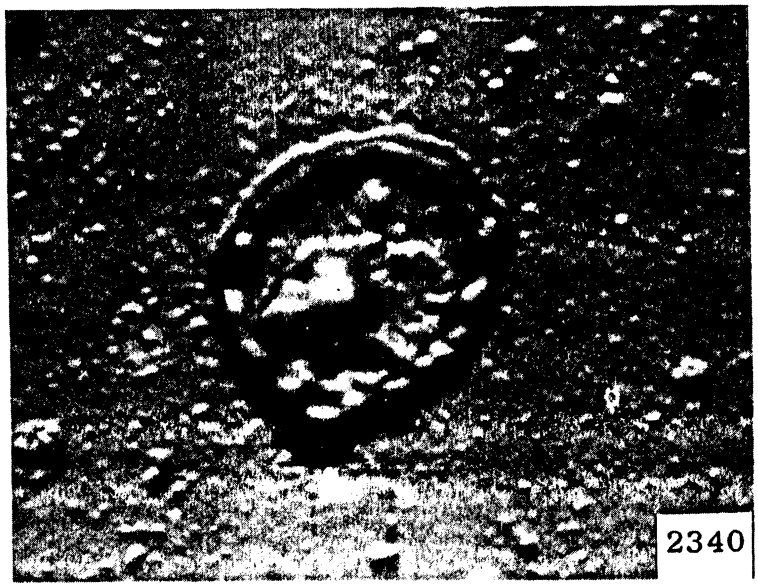

(a)

Figure 8. Crater produced by cavitating water in University of Michigan venturi on plexiglass, magnification 4,000x. (#2340)

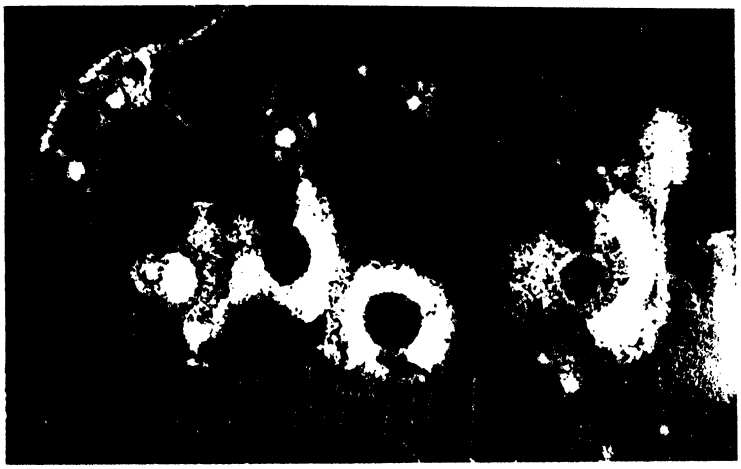

A

Coating Thickness: 2.5×10^{-5} in.

(120x)

Figure 9. Craters produced by cavitating water on 0.6 um cadmium-plated stainless steel. University of Michigan venturi.

(#2825)

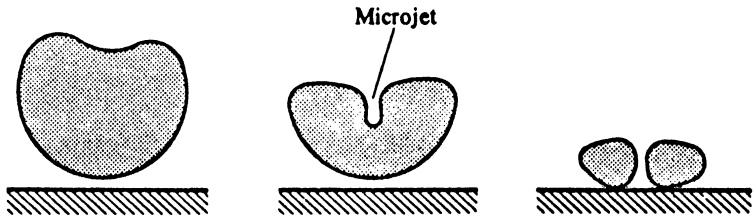

Figure 10. Schematic representation of successive stages of non-symmetrical cavity collapse with microjet impingement against a metallic surface.

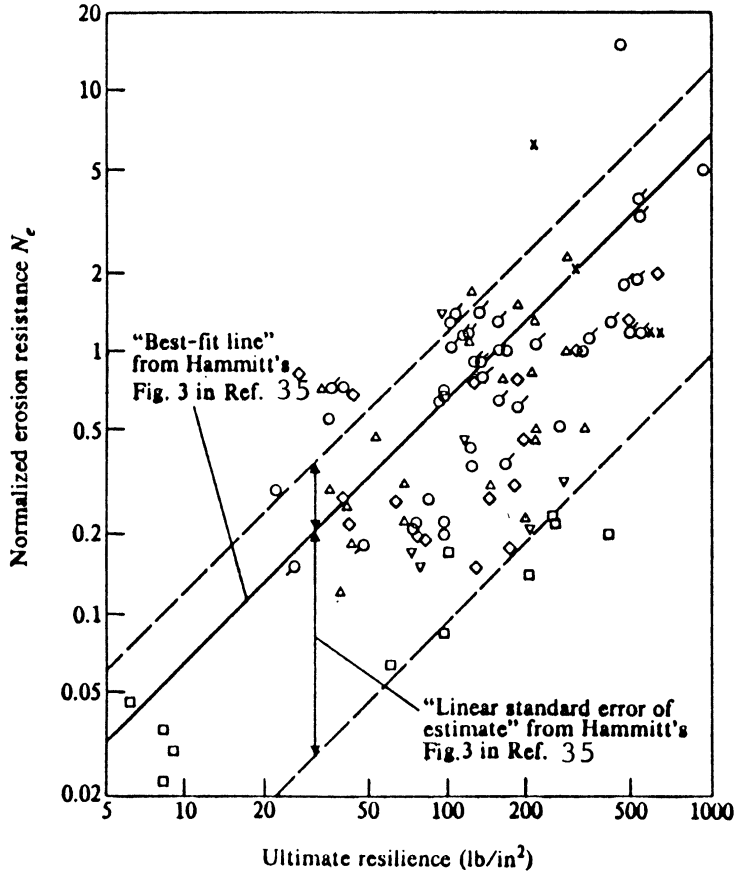

Figure 11. Erosion resistance vs. ultimate resilience: Comparison of Hammitt and Heymmann correlations.

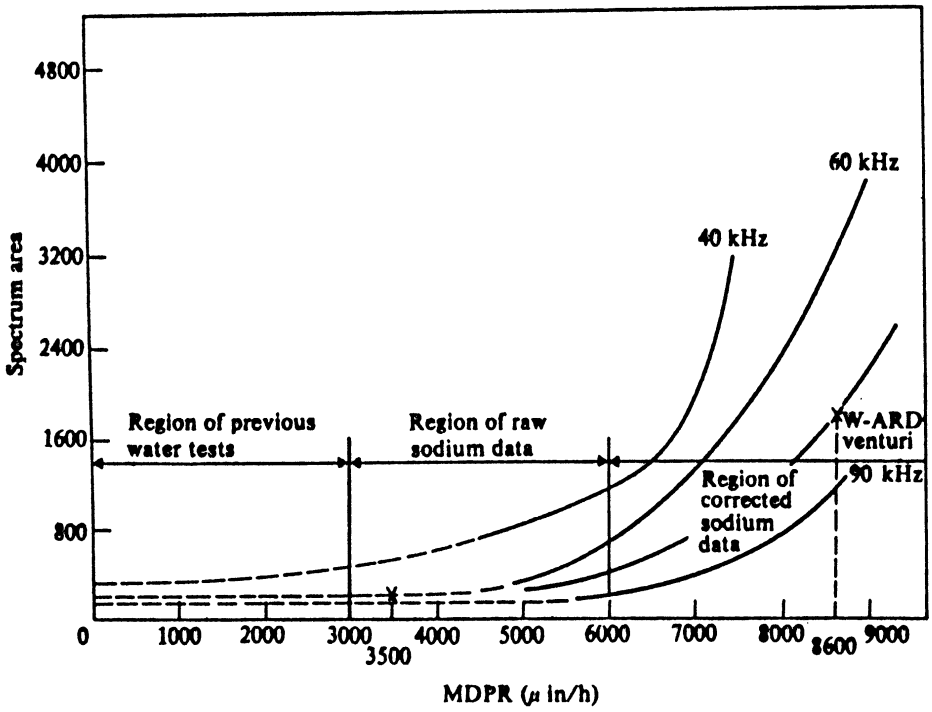

Figure 12. Correlation of bubble collapse pulse spectrum and cavitation erosion rate. (#811)

Figure 13. Acoustic power vs. erosion power for 1100-0 Aluminum (#5502) in venturi.

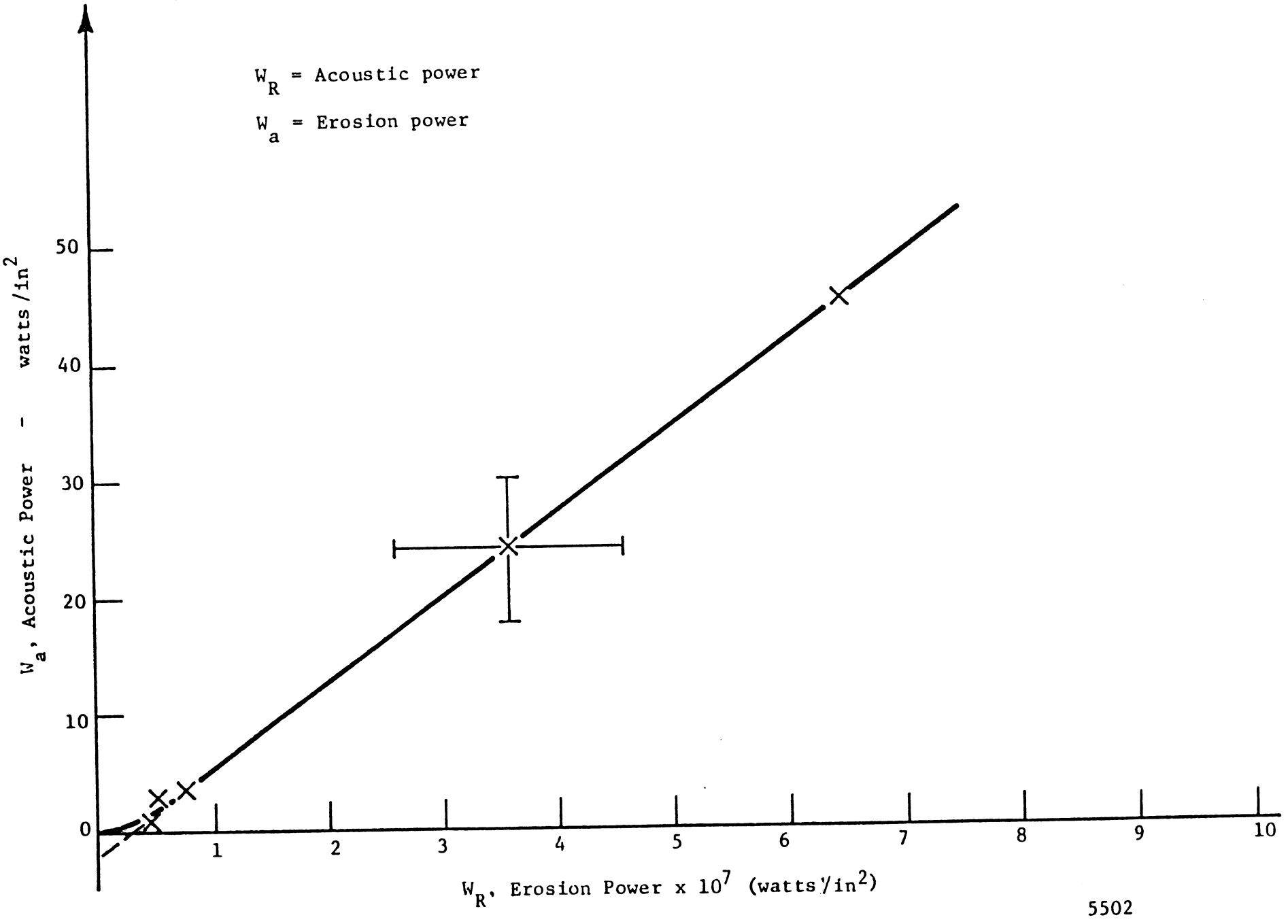

Figure 14. Number of counts per minute vs. pressure.
(Venturi, Spec, #11, 49 m/s) (#5503)

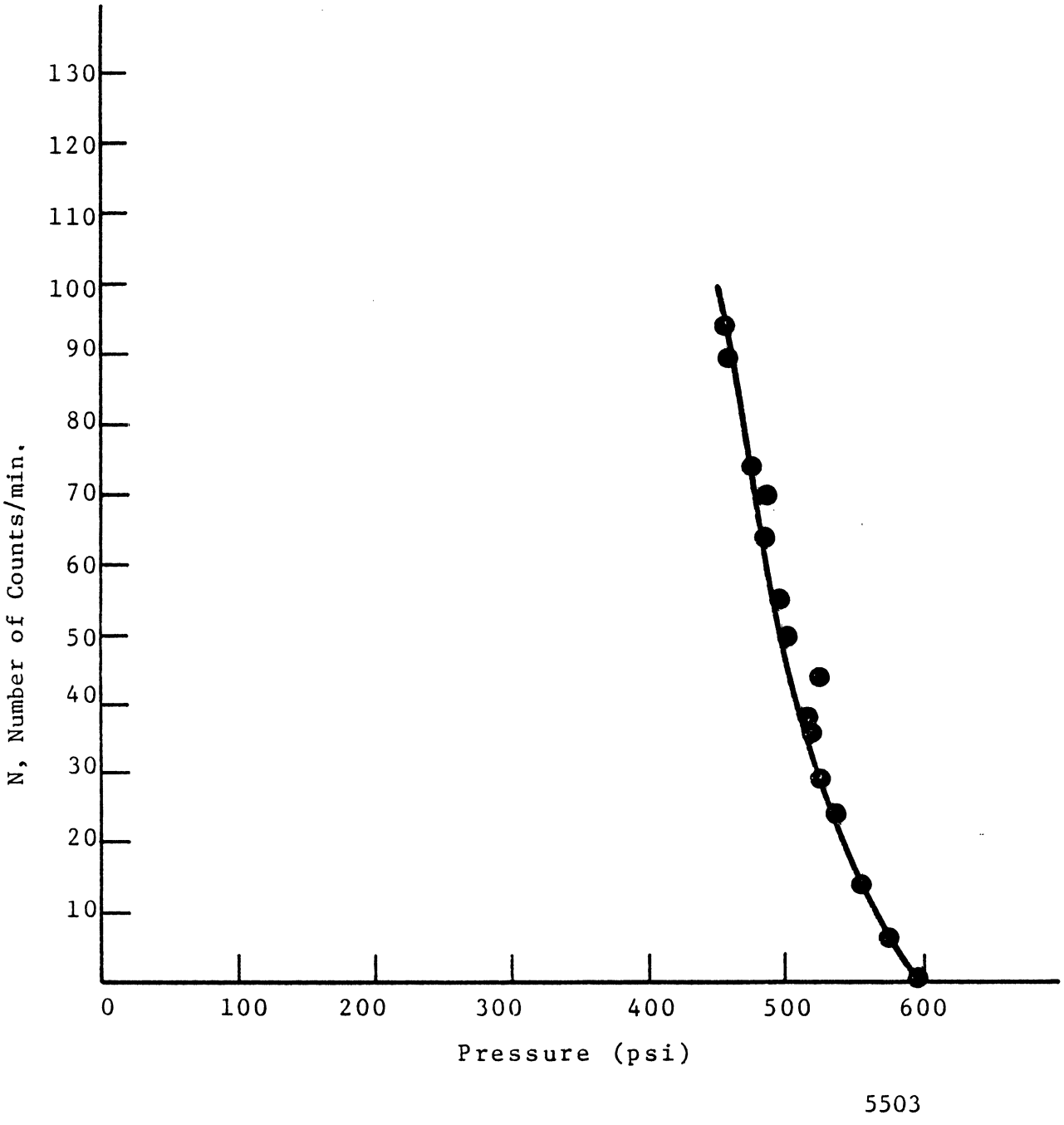

Figure 15. Differential pressure pulse height distribution (Specimen #11, 49 m/s Venturi) (#5504)

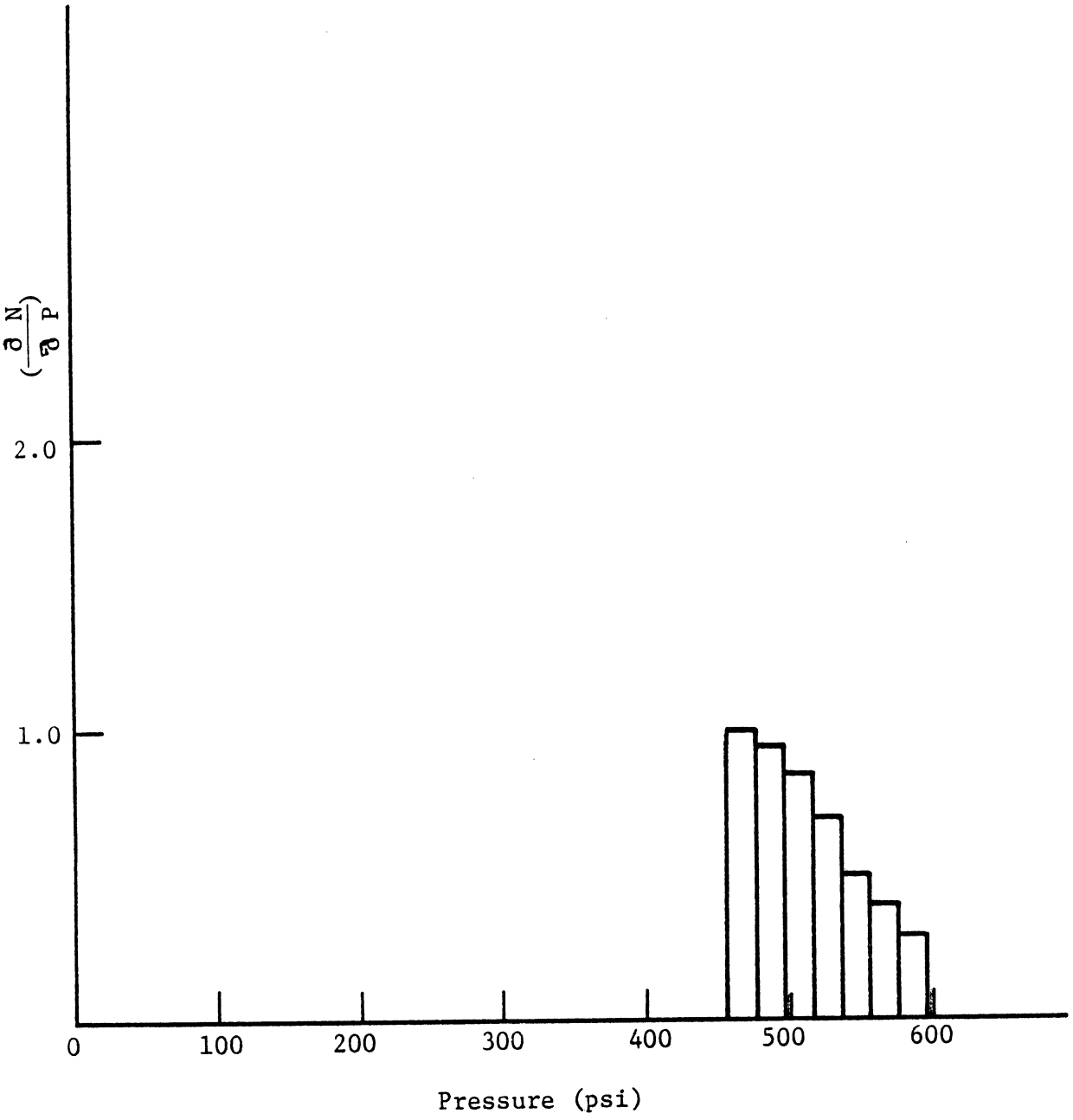

Figure 16. Differential pressure-squared pulse height distribution. (Specimen #11, 49 m/s Venturi) (#5505)